Sensors and Materials, Vol. 11, No. 2 (1999) 071–086
MYU Tokyo

S & M 0357

A High-Yield Drying Process for Surface-Micromachined Structures Using Magnetostatic Forces

Chang Liu, Thomas Tsao[1] and Yu-Chong Tai[1]

Microelectronics Laboratory, University of Illinois at Urbana-Champaign,
Urbana, IL 61801, USA
[1]Department of Electrical Engineering, California Institute of Technology,
Pasadena, CA 91125, USA

(Received December 18, 1997; accepted December 4, 1998)

Key words: magnetic actuation, surface micromachining, stiction prevention

Etching of sacrificial material is widely used in surface micromachining technology to form integrated micromechanical structures. The process typically consists of three steps: the removal of sacrificial-layer material using liquid chemicals, rinsing, and removal of the rinse liquid (drying). The last step is known to cause surface sticking and drastic reduction of device yield. This paper presents the latest results on the development of a novel drying technique in which surface microstructures are lifted away from the substrate plane during the liquid-removal process to avoid contact and sticking with the substrate. Electroplated Permalloy material is employed to provide torque to the microstructure through interaction with an external magnetic field. This method is especially useful for microdevices with large surface areas. Test structures with contact-surface areas larger than 1×1 mm^2 are fabricated to demonstrate the high yield (100%) achievable using this technique.

1. Introduction

Micromachining technology and micro-electromechanical systems (MEMS) have been undergoing dynamic development in the past 15 years.[1,2] MEMS offers unique advantages including miniaturization, mass fabrication and monolithic integration with microelectronics. It has enabled successful demonstration of novel sensors, actuators and systems in many diverse application areas such as optics,[3] fluid mechanics,[4] biomedical

engineering, communication and information storage. The characteristic length scale of micromachined devices ranges from micrometer to centimeter.

Surface micromachining is a major branch of micromachining technology. It is widely used for development of MEMS because it is highly compatible with existing integrated circuit processes. A thin-film sacrificial layer is first deposited on the wafer followed by other structural thin films on top of it. After patterning structure layers, the sacrificial layer is selectively removed to free top-level structures. The removal of the sacrificial layer can be achieved using either wet chemical etch or dry etching (plasma-based etching.) The wet etching is widely used because of its high speed and simplicity. As an example, a common process utilizes polycrystalline silicon as the structural layer and phosphosilicate glass (PSG) as the sacrificial material; the PSG material can be selectively removed using liquid hydrofluoric acid.

Liquid-phase sacrificial-layer etching consists of three major steps: sacrificial layer removal, rinsing, and the removal of the rinse liquid. The first two steps typically have high yields. The ensuing drying process, however, can potentially cause significant loss of yield due to contact and sticking of solid surfaces. At the start of the drying process, a microstructure, *e.g.*, a microcantilever beam, is completely immersed in the rinse liquid (Fig. 1(a)). As the liquid content is gradually removed through evaporation, the top surfaces of microstructures are exposed to air first; a small amount of rinse liquid is trapped underneath the suspended structure and evaporates at a much slower rate. This trapped liquid body induces surface tension at its interface with air; consequently, a pull-down force is applied to the microstructure. Since most surface-micromachined structures are located near the substrate (with a typical spacing of only a few micrometers as defined by the thickness of the sacrificial layer) and are generally very compliant, the pull-down force is capable of drawing the structure into contact with the substrate (Fig. 1(b)). Once the contact is established, solid surfaces may strongly adhere to each other due to chemical bonding or electrostatic forces. This bonding causes device failure and drastically reduces the device yield.[5–8]

Previously reported techniques to improve the yield in the drying process involve the use of several methodologies. First, unique postrelease chemical treatments are used to alter the chemical composition of the surface layer[7,9] and to reduce the bonding energy between surfaces that are in contact. Each method is useful for a selected set of structure and sacrificial-layer materials. Second, a freeze/sublimation process[10–12] can replace the liquid-to-vapor phase transformation, which is the cause of the surface tension. This method is very effective; unfortunately, it requires the use of dedicated equipment and materials. Third, microstructures can be separated from the substrate during release/drying using polymer columns which are subsequently removed using a plasma etch.[13–14] Other novel techniques utilize (1) geometric modifiers along the periphery of microstructures,[8] (2) increased temperature of the rinsing liquid,[8,10] (3) pulsed Lorentz force for re-releasing stuck structures,[15] (4) roughened surface with reduced contact area,[16] and (5) gas-phase etchants.[17] Recently, Kim and Kim[18] cross-examined a number of the above-mentioned techniques.

In many MEMS applications, large surface areas (typically $> 1 \times 1$ mm^2) are required. For example, in fluid control applications, microstructures must have adequate surface

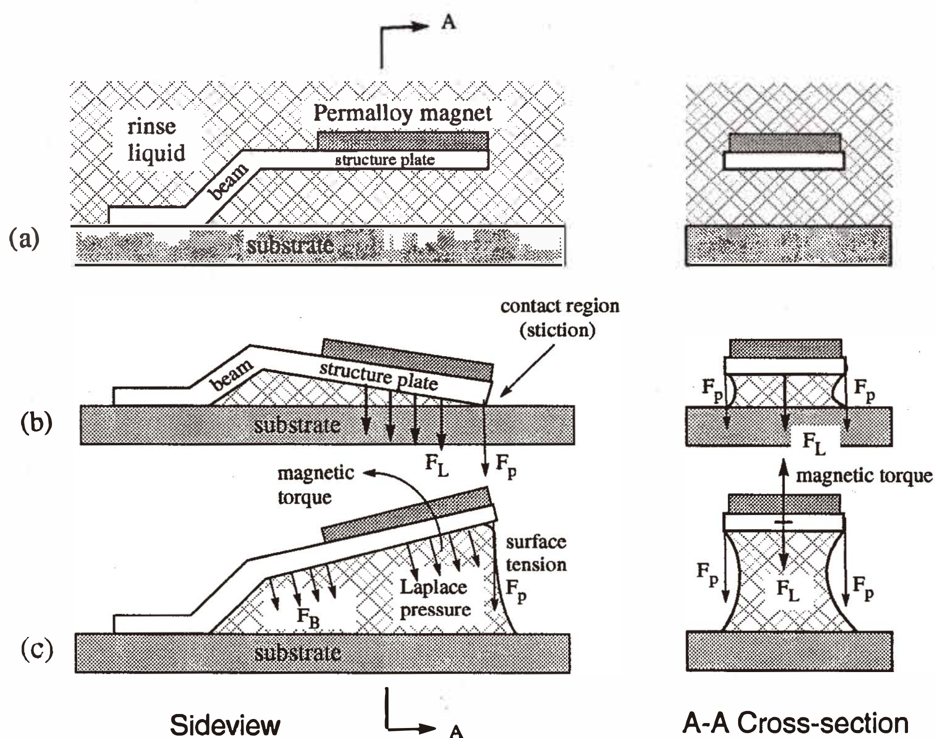

Fig. 1. Schematic diagram of the drying process. (a) Before the drying process starts, test structures are immersed in liquid and are parallel to the substrate surface; (b) surface-tension forces (F_P, F_L and F_B) draw microstructures into contact with the substrate; (c) with the active levitation by magnetic actuation, the structure is separated from the substrate.

areas to effectively interact with macroscopic fluid flow. In micro-optical systems, devices with large surface areas are frequently used as binary lenses, gratings, and mirror elements. For these structures, the probability of damage from stiction increases with increasing areas of surface contact. Many of the above-mentioned antistiction techniques (*e.g.*, surface chemical treatment) only reduce the surface bonding energy but do not completely eliminate the risk of surface bonding. These have limited success when dealing with microstructures with large surface areas.

We have developed a new technique for reducing the risk of stiction and increasing process yield. Such a method is relatively simple to implement and especially beneficial for devices with large surface areas. A magnetic thin film (*e.g.*, Permalloy) is integrated with microstructures (Fig. 1(a)), which contain thin-film plates and support beams, both of which are made of nonmagnetic material (*e.g.*, polycrystalline silicon). The attached magnetic piece can interact with an externally applied magnetic field and provide a torque,

which always tends to align the magnetization vector with the field lines (Fig. 1(c)). The microstructure and the substrate are actively separated by the magnetic torque during the drying of the liquid, thereby eliminating contact and sticking of solid surfaces. After the rinse liquid is completely removed, the magnetic field is removed and microstructures are returned to the substrate plane. Magnetic levitation provides the following advantages: (1) it can satisfy the requirements of large displacement (above 30° angular displacement) and large forces (on the order of 100 μN) simultaneously; (2) it can be achieved globally using an externally applied magnetic field, thereby enhancing the efficiency when a large number of microstructures are involved.

2. Mechanism

2.1 *Magnetostatic interactions*

The interaction between the Permalloy piece and the external magnetic field is briefly described as follows. When the external magnetic field is zero, the Permalloy material is not magnetized (with the magnetization being zero). An internal magnetization, denoted M, develops within the Permalloy once an external magnetic field is applied. For the test structure diagramed in Fig. 2, the orientation of M is within the plane of the structure plate. The magnitude of M depends on the externally applied magnetic field. As the magnetic force, H, increases, the magnitude of M grows until the saturation magnetization M_s is reached (assuming that H and M are along the same direction). The measured relationship between the external magnetic force and the magnetization is shown in Fig. 3.

The magnitude of M also depends on the angle between M and H. Comprehensive analysis between the angular displacement and the external magnetic field has been conducted in the past.[19,20] In this application, we are mainly concerned with situations wherein the displacement is greater than 20° and the magnetization has become saturated.

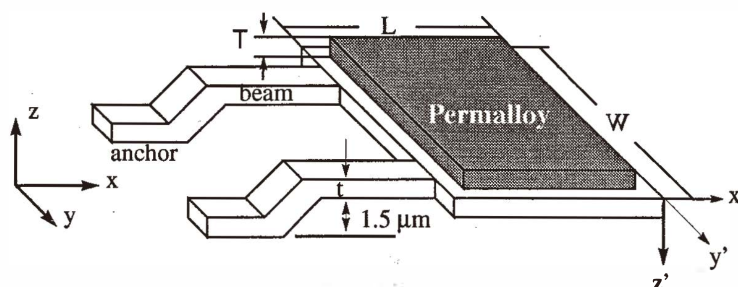

Fig. 2. A schematic perspective view of a test structure. A Permalloy piece is placed on top of a microplate which is supported by two cantilever beams. The spacing between the plate and the substrate is 1.5 μm.

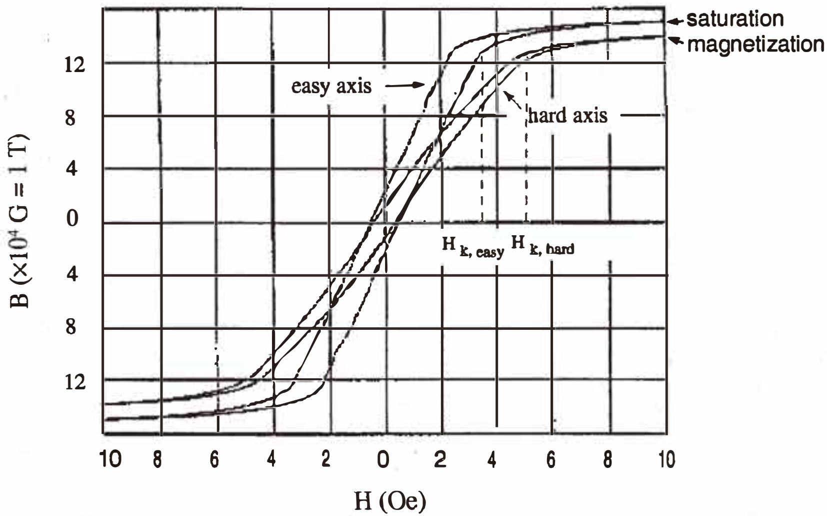

Fig. 3. Calibrated *B-H* loop (in both easy and hard axes) of the Permalloy thin film.

If we simply treat the Permalloy material as having a fixed in-plane magnetization with its magnitude equal to M_s, the torque acting on the Permalloy piece, M_{mag}, can be expressed as a function of the angular displacement, θ:

$$M_{mag} = M_s H(WTL)\cos\theta \tag{1}$$

where M_s is the saturation magnetization of the magnetic material, the terms W, L and T are the width, length, and thickness of the Permalloy piece, respectively (Fig. 2). The product of W, L and T is the volume of the Permalloy piece.

2.2 *Forces due to surface tension*

The surface tension between the rinse liquid and the air contributes to the pull-down force experienced by the test structure. The pull-down force consists of three components (Fig. 4), including distributed Laplace pressure (F_L), distributed surface tension forces along the perimeter of the structural plate (F_P), as well as distributed forces along the length of the cantilever beams (F_B). The Laplace pressure is proportional to the sum of the inverse of the radii of curvatures associated with the liquid-air interface. The overall magnitude of the generated torque contributed by surface tensions will decrease as θ increases. In the test structures in this study, the component F_p contributes most significantly to the magnitude of the surface tension force. Assuming that surface tension forces act along the entire perimeter of the suspended structural plate, the overall torque produced by F_p with

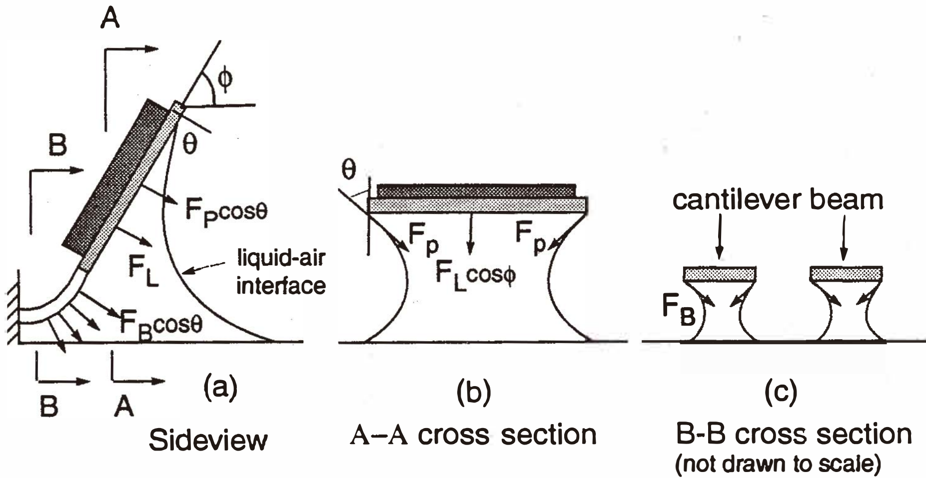

Fig. 4. Schematic diagram of surface tension forces (a) the side view, (b) A-A cross-sectional view and (c) B-B cross section.

respect to the free end of the cantilever beams is estimated as

$$M_{st} = \gamma(WL + \frac{1}{2}L^2)\cos\theta\cos\phi, \tag{2}$$

where $W = L = 1$ mm are the width and the length of the microstructure, respectively. The term (is the surface tension of the liquid-air interface. The term ϕ represents the angle between the normal direction of the structural plane and the tangential plane of the liquid at the point of contact. The magnitude of M_{st} decreases as the angular displacement is increased. The magnitude of the angle ϕ, however, is difficult to predict. Its value changes with diminishing amount of trapped liquid. In the first order analysis, we treat ϕ as a constant to simplify the analysis.

2.3 *Equilibrium position*

Before the start of drying, the microstructure is immersed in a liquid solution. No surface tension forces act on the microstructure at this moment. The magnitude of the torque contributed by the elastic bending of the microstructure, M_e, is expressed as

$$M_e = \frac{EI\theta}{l}, \tag{3}$$

where E is the Young's modulus and I the moment of inertia of the support beam. Upon the application of a DC magnetic field H, the structure reaches an equilibrium position, θ_1, determined by the following torque balance equation:

$$M_{mag} = M_e = M_s WTLH \cos\theta_1 = \frac{\alpha EI\theta_1}{l}. \quad (4)$$

The term α is a constant; it accounts for displacement due to force and variation of parameters such as E and M_s. As the liquid solution is gradually removed, the surface tension force develops. The microstructure reaches a second equilibrium position (Fig. 4(a)), determined by the torque balance:

$$M_{mag} = M_e + M_{st}. \quad (5)$$

Using eqs. (1), (2), and (3), the above torque balance equation can be written as

$$M_s WTLH \cos\theta_2 = \frac{EI\theta_2}{l} + \gamma(WL + \frac{1}{2}L^2)\cos\theta_2 \cos\phi, \quad (6)$$

where θ_2 is the new equilibrium position ($\theta_2 < \theta_1$). As the liquid is gradually removed, the magnitude of M_{st} will decrease because the liquid is in contact with a smaller area of the microstructure. The equilibrium angle θ will therefore increase from θ_2 to θ_1. In order to prevent microstructures from being pulled to come into contact with the substrate, two conditions must be met: (1) the solution to eq. (6) must exist and (2) the initial displacement θ_1 must be greater than θ_2.

For a given microstructure and rinsing fluid, it is of interest to determine the minimum initial displacement θ_1 and the external magnetic field that are required to successfully implement this new drying method. The lifting method will be successful as long as the initial displacement, θ_1, is above a certain threshold. If the θ and H are below the threshold value, eq . 6 will have no solution and the microstructure will be pulled to the substrate. To determine the value of the threshold θ_1 and H, we apply iterative calculations. An initial value for H is assigned arbitrarily. The value of θ_1 can be determined using eq . (4). A non-zero solution of θ_2 is then solved numerically using the transcendental eq. (6). If the solution does not exist, the value for H is raised. If a solution exist, the magnitude of H is systematically decreased and the previously specified procedure is repeated until the minimum solution for H and the related θ_1 are found.

2.4 *Test structures*

The test structure under study contains a square plate supported by two cantilever beams (Fig. 2). The plate and support beams are both made of thin-film polycrystalline silicon. An electroplated Permalloy magnetic piece is located on top of the plate. Scanning electron micrographs of fabricated test structures are shown in Fig. 5. The cantilever beam

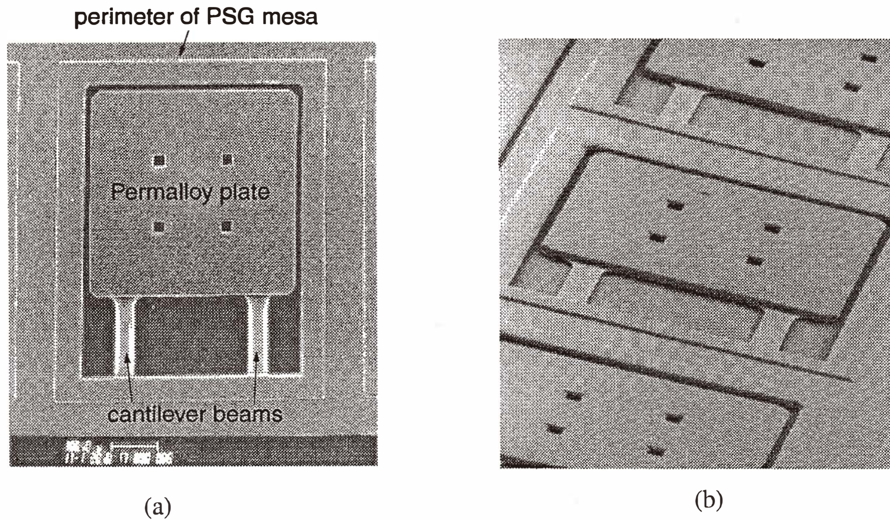

(a) (b)

Fig. 5. SEM images of (a) top view and (b) perspective view of a test structure. The area of the Permalloy piece is 1 mm × 1 mm; the thickness is 5 μm.

is 400 μm long and 100 μm wide; its thickness ranges from 2,100 nm to 1.5 μm. The plate has a surface area of 1×1 mm^2; its thickness is the same as that of the support beams. The electroplated Permalloy pieces have a thickness ranging from 1 to 5 μm; in our test structures, these have the same area as the plate. A large number of test structures (100 on a 1×1 cm^2-sized chip) is used to produce reliable statistical figures for the yield.

3. Materials and Methods

3.1 *Magnetic properties of the Permalloy material*

The electroplated Permalloy has a composition of 80% nickel and 20% iron.(21) Thin film Permalloy is the preferred soft magnetic material with negligible level of intrinsic stress. The experimental *B-H* hysteresis curves along the easy axis and the hard axis are shown in Fig. 3. During the NiFe electroplating, the direction of the biasing magnetic field dictates the orientation of the easy axis.(21,22) The direction parallel to the external magnetic field during the plating process is the easy axis while the orthogonal in-plane direction is the hard axis. This phenomenon has been studied by Takahashi;(22) it has been found that an external field of H = 2,400 A/m is sufficient to induce directional order. The Permalloy material used in this study shows only a minor difference in magnetic behavior between easy and hard axes. The properties of the electroplated magnetic material are summarized in Table 1.

Table 1
Summary of properties of the thin-film Permalloy material.

Property	Value
Saturation magnetization M_s	1 – 1.5 T
Coercive force H_c	0.6 Oe (47 A/m)
Relative permeability μ_r	4,500

3.2 *Test structure fabrication*

The fabrication process for a typical magnetic actuator is summarized in Fig. 6. The entire process is divided into five steps.

Step 1 (Fig. 6(a))

A 3-μm-thick phosphosilicate glass (PSG) thin film is first deposited on top of the silicon substrate at 450°C. The thin film functions as a sacrificial material. After removal of the photoresist layer, the wafer is annealed in nitrogen ambient at 1000°C for one h. This step serves two purposes. First, it activates the phosphorus dopant (6 wt.%) within the PSG layer and increases its etch rate by buffered hydrofluoric acid (BHF). Second, the PSG material reflows slightly at the temperature of the oxidation, creating a rounded, smooth profile along the perimeter of the PSG mesas. The wafer is then covered by a highly conformal deposition of thin polycrystalline silicon using low-pressure chemical vapor deposition techniques (LPCVD).

A 0.5-μm-thick PSG layer is then deposited on top of the polysilicon. It serves as a complimentary doping source. During a 1-h, 950°C stress-relief anneal in nitrogen ambient, the polysilicon is doped symmetrically from both sides. The symmetric doping reduces the intrinsic stress gradient across the thickness of the polysilicon and minimizes residue beam bending. The SEM images shown in Fig. 3 show no intrinsic bending in the test structures. In contrast, doping from only one side would generate a non-symmetric doping concentration and a stress gradient. The top PSG layer is later removed using BHF.

Step 2 (Fig. 6(b))

The thermally-evaporated seed-layer, containing 200-Å-thick Cr and 1800-Å-thick Cu thin films, is deposited on the front side of the wafer as a seed-layer. The thickness of this layer must be sufficient to ensure electrical continuity throughout the wafer. We apply a 5-μm-thick photoresist layer to prevent the copper film from oxidizing in air. The photoresist is patterned and developed only immediately before electroplating.

Step 3 (Fig. 6(c))

Patterned photoresists form narrow frames. In regions that are not covered by the photoresist, the seed-layer is exposed and Permalloy ($Ni_{80}Fe_{20}$) electroplating takes place. In the electroplating process, an external biasing magnet (3.6×10^4 A/m) is applied with

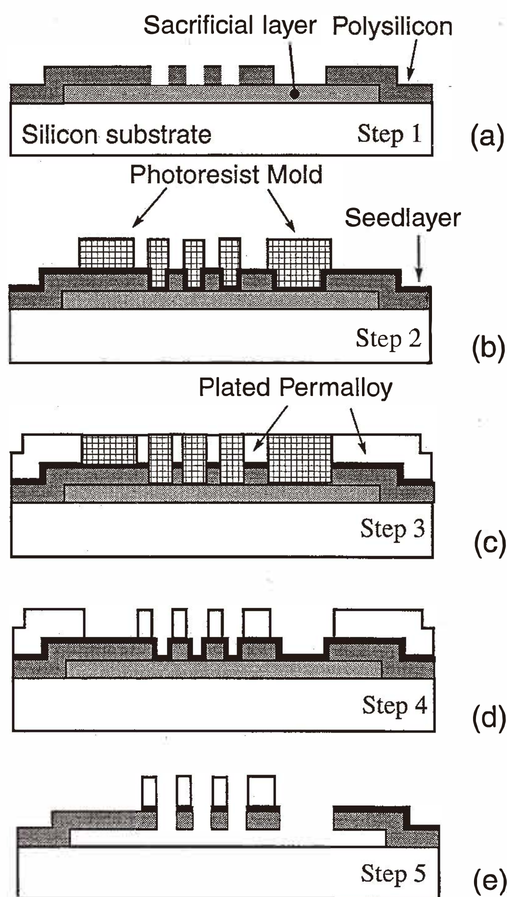

Fig. 6. The fabrication process for the test structures.

the field lines being parallel to the wafer substrate. This bias establishes the easy axis within the Permalloy piece. Electroplating takes place at a rate of 5 μm/h under a bias-current density ranging from 8 to 12 mA/cm^2.

Step 4 (Fig. 6(d))

After electroplating, the wafer is flooded with ultraviolet radiation and the photoresist is removed with a standard photoresist developer. The wafer is further cleaned using acetone and then isopropanol solutions.

Step 5 (Fig. 6(e))

The exposed seed-layer is removed using Cu etchant (100:5:5 wt. water:acetic acid: hydrogen peroxide) and then a Cr-mask etchant. It typically requires 10 s to remove the Cr layer using diluted HCl. Occasionally, etching of Cr does not occur spontaneously; namely, the Cr layer stays intact even when the wafers are immersed in Cr etchants for up to 100 times the nominal etching time. This phenomenon is believed to result from an unfavorable electrochemical potential on the wafer. To solve this problem, the electrochemical potential of the seed-layer is modified by contacting the Cr layer with a piece of pure aluminum.

Fabricated test structures were first immersed in HF solution (49% wt.) to fully remove the sacrificial material located beneath the structural layers. To facilitate the sacrificial-release process, etch holes (30 μm by 30 μm in area, and 250 μm apart) are uniformly distributed on the plate. The Permalloy material withstands HF etching without damage.

4. Results

Following the last step in the fabrication process, wet wafer dies are transferred directly to deionized (DI) water bath and fully rinsed to remove remaining chemical solutions. Dies are then immersed in a final rinse solution for 10 min. Chemicals with low surface tension (*e.g.*, isopropyl alcohol and methyl alcohol) are preferred. The wet dies are dried in air using a setup shown in Fig. 7. We first apply the external magnetic field and lift the structural plates to an equilibrium displacement angle (θ_1) when the structure is fully immersed in liquid. The angular displacement of the microstructure in an external magnetic field is governed by eq . (3); it has been fully characterized experimentally (Fig. 8) for a test structure with Permalloy plate thickness of 5 μm. The result of the analysis (eq. (3)) and experiments agree well.

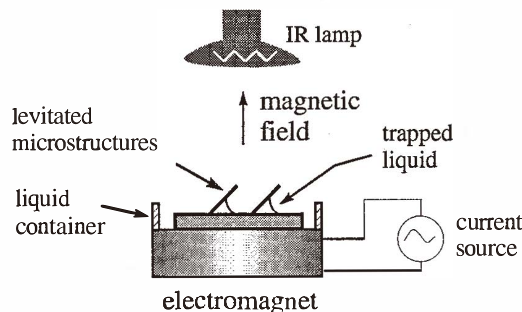

Fig. 7. The experimental drying setup. A test chip with microstructures is placed on top of an electromagnet and an infrared lamp is used to increase the evaporation speed.

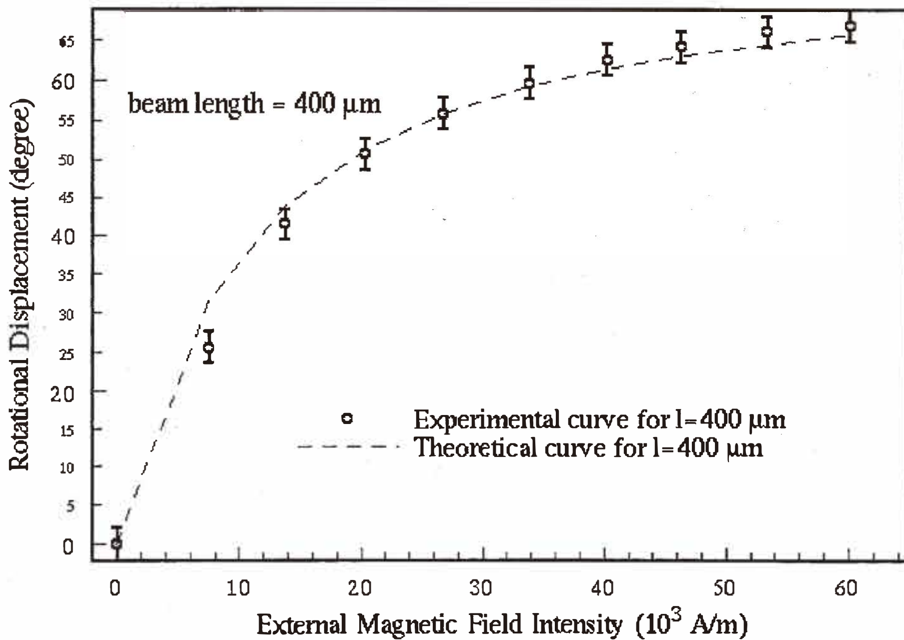

Fig. 8. The angular displacement of a microstructure as a function of the external magnetic field strength. The thickness of the Permalloy piece is 5 μm.

The microstructure is first lifted to θ_1 = 65°, under a biasing magnetic field of H = 60,000 A/m (Fig. 8). Using the experimental finding, the constant α in eq. (4) is determined as 2.8 given that M_s = 1.5 T and $E = 1.6 \times 10^{11}$ Pa. As the liquid on top of the microstructure is removed, the new equilibrium position becomes θ_2 = 60° (Fig. 9(a)). Figure 9 is a sequence of captured video images showing the side profile of the test structure and the trapped liquid (in diminishing amounts from Fig. 9(a) to Fig. 9(c)). Notice that the rinse liquid significantly reduces the contrast in the images. Infrared heating is applied to accelerate the liquid removal process (Fig. 9(b)). When the liquid is completely removed, the displacement of the structure is again θ_1 = 65°. There are two additional features. First, the radius of curvature of the liquid-air interface in the vertical planes decreases from Fig. 9(a) to Fig. 9(b). Second, the liquid-covered area on the back of the plate decreases as the liquid is evaporated.

The result shows that 100% yield is routinely achieved using θ_1 = 65. As a comparison, we have found that less than 10% yield is achievable when no magnetic levitation is used. Several rinse solutions (including isopropyl alcohol, methyl alcohol and water) work well, although a longer drying time is needed when DI water is used. (The surface tension of water is more than 3 times greater than that of an alcohol solution.) The complete process is summarized in Table 2.

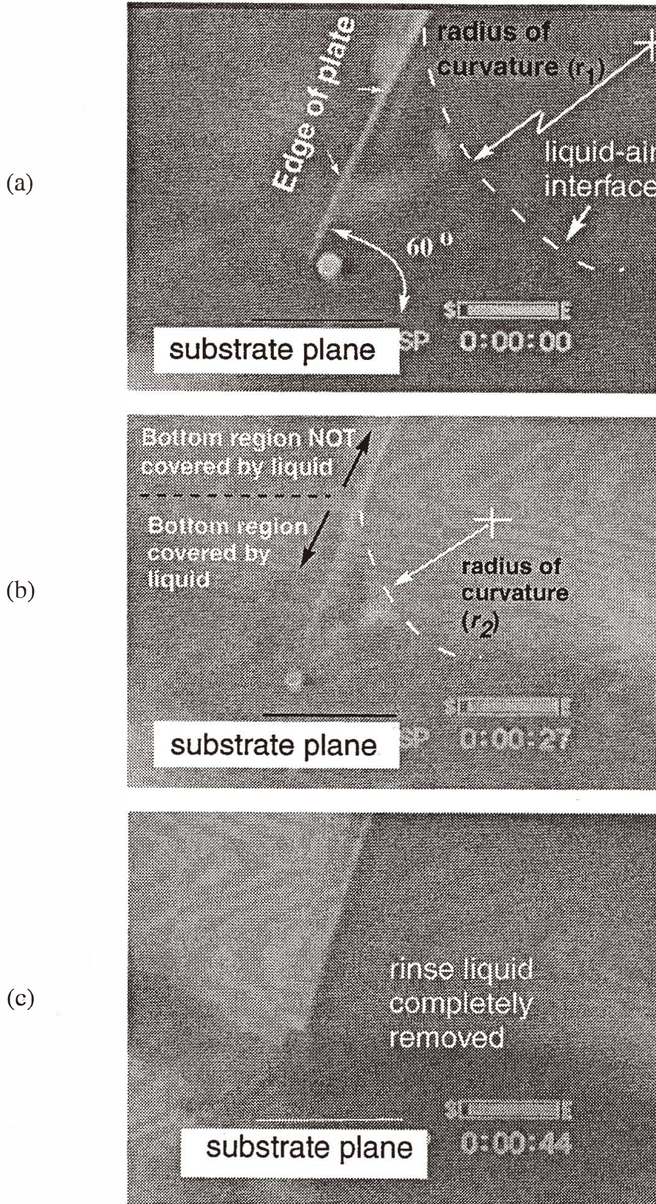

Fig. 9. A sequence of three video images showing the side view of a plate and the liquid-air interface (dotted lines) during three phases of drying. (a) Profile of the plate and the liquid-air interface after the front surface of the plate is exposed to air; the radius of curvature is r_1. Liquid covers the entire bottom surface of the plate. (b) Profile after the liquid is partially evaporated; the radius of curvature, r_2, is smaller than r_1. Liquid covers only a part of the bottom surface of the plate. (c) Profile of the plate after the liquid is completely removed. The final rinse solution is isopropanol alcohol.

Table 2
The process for drying surface-micromachined devices.

Step	Process description
1	Etch in 49% HF solution until full release.
2	Rinse in DI water for 5 min.
3	Rinse in a final rinse solution for 10 min.
4	Direct transfer to drying setup shown in Fig. 4.
5	Apply heat (for evaporation) and magnetic field (for levitation).
6	Remove heat and magnetic field after solution is evaporated.

Using eq. (6), it is found that the surface tension is approximately 66 mN/m by setting the contact angle to $\phi = 0°$. Using the procedure outlined in Section 2.3, we find the minimum required magnetic field H to be 1.38×10^4 A/m. The first equilibrium position is $\theta_1 = 30.6°$. We also experimentally determined the minimum required magnetic field that allows successful drying. The experiment contains iterative steps in which the microstructure is first raised to a certain angle in liquid followed by liquid removal. The magnetic field is reduced until the microstructure is stuck to the surface during the drying process. The minimum magnetic field found using this method is 1.60×10^4 A/m, which corresponds with the analysis well. We speculate that the error is contributed by three sources: (1) other surface tension components that were neglected in eq. (2); (2) other forms of forces (such as molecular forces); and (3) value for the contact angle, ϕ.

5. Discussions

Although the integration of magnetic material with the polysilicon microstructures adds one more step to the overall fabrication process, the drying procedure is straightforward and does not involve complex chemical or mechanical treatments. The fabrication process for a regular surface micromachined device generally follows steps a and d of Fig. 6. Steps b, c and d are associated with the magnetic-assisted release/drying technique. The added steps are relatively simple and accessible, requiring only one extra mask for patterning the Permalloy material.

In current test structures, the area of the Permalloy material is identical to that of the structure plate. However, the Permalloy piece is not required to cover the entire structural plate. By reducing the size of Permalloy pieces, the material can be less intrusive to the intended functions of the microdevices. It is also feasible to develop polymer-based magnetic material that can be removed by plasma etching.

6. Conclusions

We have demonstrated a high-yield method of releasing surface micromachined structures. Using active magnetic levitation, surface-micromachined structures are kept away from the substrate during the drying process to prevent contact between the structure and the substrate. This technique is intended to supplement existing antistiction methods. It is especially useful for devices that have large surface areas. This technique is limited to cases where microstructures can achieve angular deflection. A high yield of 100% has been routinely demonstrated for structures as large as 1×1 mm^2. Analysis of the torque balance during the drying process has yielded a procedure for determining the minimum required magnetic field and initial displacement for ensuring successful drying.

Acknowledgement

This work was supported by DARPA. The authors wish to thank Mr. Shuyun Wu at the California Institute of Technology for technical discussions and processing assistance.

References

1 H. Fujita: Proceedings, IEEE Workshop on Micro Electro-Mechanical Systems (IEEE, Nagoya, 1997) p. 1.
2 K. Petersen: Proc. IEEE 70 (1982) p. 420.
3 S. S. Lee, E. Motamedi and M. C. Wu: Tech. Digest., 1997 International Conference on Solid-State Sensors and Actuators (Chicago, 1997) p. 85.
4 C. M. Ho. and Y. C. Tai: Journal of Fluid Engineering (Sept. 1996) 437.
5 C. H. Mastrangelo and C. H. Hsu: IEEE Solid-State Sensor and Actuator Workshop (Hilton Head Island, SC, 1992) p. 208.
6 R. Legtenberg, J. Elders and M. Elwenspoek: Proceedings, 1993 International Conference on Solid-State Sensors and Actuators, Transducer'93 (1993) p. 198.
7 R. L. Alley, G. J. Cuan, R. T. Howe, *et al.*: IEEE Solid-State Sensor and Actuator Workshop (1992) p. 202.
8 T. Abe, W. C. Messner and M. L. Reed: Proceedings, International Workshop on Micro Electro Mechanical Systems 1995, MEMS'95, p. 94.
9 M. R. Houston, R. Maboudian and R. T. Howe: Proceedings, 1995 International Conference on Solid-State Sensors and Actuators, Transducer'95 (1995) Vol. I, p. 210.
10 T. Abe, W. C. Messner and M. L. Reed: Journal of MEMS **4** (1995) 66.
11 G. T. Mulhern, D. S. Soane and R. T. Howe: Proceedings, 1993 International Conference on Solid-State Sensors and Actuators, Transducer'93 (1993) p. 296.
12 N. Takeshimo, *et. al.*: Proceedings, 1991 International Conference on Solid-State Sensors and Actuators, Transducers'91 (1991) p. 63.
13 C. H. Mastrangelo and G. S. Saloka: Proceedings, IEEE Workshop on MEMS, MEMS'93 (IEEE, Oiso, 1993) p. 77.
14 M. Orpana and A. O. Korhonen: Proceedings, 1991 International Conference on Solid-State Sensors and Actuators, Transducers'91 (1991) p. 957.
15 B. P. Gogoi and C. H. Mastrangelo: Proceedings, 1995 International Conference on Solid-State Sensors and Actuators, Transducer'95, Vol. I (1995) p. 214.

16 Y. Yee, K. Chun and J. D. Lee: Proceedings, 1995 International Conference on Solid-State Sensors and Actuators, Transducer'95 (1995) p. 206.
17 J. H. Lee, Y. I. Lee, W. I. Jang, *et al.*: IEEE Workshop on Micro Electro Mechanical Systems, MEMS 97 (IEEE, Nagoya, 1997) p. 448.
18 J. Y. Kim and C. J. Kim: IEEE Workshop on Micro Electro Mechanical Systems, MEMS 97 (IEEE, Nagoya, 1997) p. 442.
19 C. Liu, T. Tsao, P. Will, Y. C. Tai and W. H. Liu: Proceedings, International Conference on Solid-state Sensors and Actuators, Transducer'95 (IEEE, Sweden, 1995) p. 328.
20 J. W. Judy, R. S. Muller and H. H. Zappe: J. of Microelectromech. Syst. **4** (1995) 162.
21 V. Temesvary, S. Wu, W. H. Hsieh, Y. C. Tai and D. K. Miu: J. of Microelectromech. Syst. **4** (1995) 18.
22 M. Takahashi: Journal of Applied Physics, Supplement to **33** (1962) p. 1101.